Injection Induced Mixing in Flows Separating From Smooth Surfaces

David W. Wundrow
Ohio Aerospace Institute, Brook Park, Ohio

The NASA STI Program Office . . . in Profile

Since its founding, NASA has been dedicated to the advancement of aeronautics and space science. The NASA Scientific and Technical Information (STI) Program Office plays a key part in helping NASA maintain this important role.

The NASA STI Program Office is operated by Langley Research Center, the Lead Center for NASA's scientific and technical information. The NASA STI Program Office provides access to the NASA STI Database, the largest collection of aeronautical and space science STI in the world. The Program Office is also NASA's institutional mechanism for disseminating the results of its research and development activities. These results are published by NASA in the NASA STI Report Series, which includes the following report types:

- TECHNICAL PUBLICATION. Reports of completed research or a major significant phase of research that present the results of NASA programs and include extensive data or theoretical analysis. Includes compilations of significant scientific and technical data and information deemed to be of continuing reference value. NASA's counterpart of peer-reviewed formal professional papers but has less stringent limitations on manuscript length and extent of graphic presentations.

- TECHNICAL MEMORANDUM. Scientific and technical findings that are preliminary or of specialized interest, e.g., quick release reports, working papers, and bibliographies that contain minimal annotation. Does not contain extensive analysis.

- CONTRACTOR REPORT. Scientific and technical findings by NASA-sponsored contractors and grantees.

- CONFERENCE PUBLICATION. Collected papers from scientific and technical conferences, symposia, seminars, or other meetings sponsored or cosponsored by NASA.

- SPECIAL PUBLICATION. Scientific, technical, or historical information from NASA programs, projects, and missions, often concerned with subjects having substantial public interest.

- TECHNICAL TRANSLATION. English-language translations of foreign scientific and technical material pertinent to NASA's mission.

Specialized services that complement the STI Program Office's diverse offerings include creating custom thesauri, building customized databases, organizing and publishing research results . . . even providing videos.

For more information about the NASA STI Program Office, see the following:

- Access the NASA STI Program Home Page at *http://www.sti.nasa.gov*

- E-mail your question via the Internet to help@sti.nasa.gov

- Fax your question to the NASA Access Help Desk at 301–621–0134

- Telephone the NASA Access Help Desk at 301–621–0390

- Write to:
  NASA Access Help Desk
  NASA Center for AeroSpace Information
  7121 Standard Drive
  Hanover, MD 21076

Injection Induced Mixing in Flows Separating From Smooth Surfaces

David W. Wundrow
Ohio Aerospace Institute, Brook Park, Ohio

Injection Induced Mixing in Flows Separating from Smooth Surfaces

David W. Wundrow

Ohio Aerospace Institute

22800 Cedar Point Road

Brook Park, Ohio 44142

Email: David.W.Wundrow@grc.nasa.gov

Abstract

An analytic model for predicting the effect of unsteady local surface injection on the flow separating from a streamlined body at angle of attack is proposed. The model uses the premise that separation control results from enhanced mixing along the shear layer that develops between the main stream and the fluid in the underlying recirculation zone [1]. High-Reynolds-number asymptotic methods are used to connect the unsteady surface injection to an instability wave propagating on the separating shear layer and then to the large-scale coherent structures that produce the increased mixing. The result is a tool that can guide the choice of fluidic-actuator parameters to maximize flow-control effectiveness and may also facilitate computer-based numerical experiments.

1   Introduction

The drive to reduce NO_x and CO_2 emissions from current and future commercial aircraft has led to an increased emphasis on improving the efficiency of turbofan engines. The performance of modern inlet/fan/compressor systems has for the most part reached the limits achievable by geometric shaping, i.e. by simply bending metal. To realize further gains, losses that occur locally within the turbomachinery blading and/or transiently during certain operating ranges must be addressed.

One common source of loss is low-momentum regions that develop along the suction sides of the aerodynamic surfaces which makeup the various engine components. In the compressor, the low-momentum regions give rise to a stall boundary which limits the amount of work obtained per stage and so dictates the number of stages required to achieve a desired pressure rise. The ability to manage this loss through adaptive flow control has now become possible due to recent advances in micro electro-mechanical systems.

Numerous experiments on isolated airfoils in cross flow and a smaller number of investigations of flow through blade cascades have demonstrated the potential of local surface injection to delay or prevent flow separation. Complementary studies using unsteady injection have shown that the same measure of flow control can be achieved with significantly less injected mass.

Limiting injected mass and thereby thermodynamic cycle penalties incurred by bleed extraction is just one of several objectives which must be considered when designing intelligent flow-control approaches for aeropropulsion systems. Additional considerations include minimizing the net injected momentum to avoid parasitic mixing losses and optimizing the acoustic characteristics of the fluidic actuator to reduce power consumption and improve frequency response.

Designing a robust effective flow-control system that maintains optimum efficiency throughout the engine operating envelope requires tailoring the actuation device for the specific environment in which it is placed. Unfortunately, parametric studies of pulsed or time-harmonic injection systems are difficult to perform experimentally (even in single blade configurations) because the useful operating range of any particular actuator is dictated by the geometries of its attendant chamber and orifice. Time-accurate numerical simulations are only marginally less difficult since altering the actuator design generally requires re-griding the problem. Similarly, the low-order models for the time-averaged effect of unsteady surface injection required by existing multi-stage steady-flow design codes are lacking.

The present investigation addresses these issues by providing an analytic model that predicts the effectiveness of separation control as a function of tunable actuator parameters. Asymptotic methods are used to formalize a mechanism for separation control proposed in reference [1] wherein the basis is mixing enhancement along the separating shear layer. The performance of a given flow-control device is measured in terms of the ratio of mass entrained by the separating shear layer to mass available in the recirculation zone. The analysis is done in the framework of the high-Reynolds-number limit which is a reasonable approximation for the flows of interest here and, in any event, often correctly captures the physical balances in play at moderate Reynolds number.

The problem is formulated in §2 where the asymptotic solution for the time-mean flow that would exist in the absence of control is given near its separation point. The unsteady flow field is analyzed in §3 where the coupling between the component forced by the surface injection and the instability wave excited on the separating shear layer is considered. In §4, a model for the enhanced mean-flow spreading rate along the shear layer is given and a flow-control metric is proposed. Some preliminary results obtained from the model are presented and their implication discussed in §5.

2 Formulation

At frequencies typical of turbomachinery applications, unsteady surface injection is thought to effect separation control through mixing enhancement. Surface injection introduces an unsteady perturbation to the flow that excites a spatially growing disturbance on the separating shear layer by the Kelvin–Helmholtz instability mechanism. The instability wave grows as it propagates downstream until nonlinear effects cause it to roll up into a discrete vortex. Further downstream, the individual vortices, which are identified with large-scale coherent structures, begin to merge and fine-grained turbulence becomes the dominant vehicle for shear-layer mixing. This evolutionary process is accompanied by enhanced entrainment of low-momentum near-wall fluid which tends to drive the separating shear layer toward the surface. If the rate of entrainment is sufficient, the streaming flow re-attaches.

The above description is cast into a workable tool for flow-control analysis by combining existing high-Reynolds-number analytic models for the following distinct fluid-mechanical phenomena that dominate various stages of the flow development: 1) the uncontrolled base flow, i.e. the time-averaged separated flow to which control is applied; 2) the linear unsteady flow field which includes the perturbation associated with the imposed surface injection and the shear-layer instability which it excites; 3) the large-scale coherent mode into which the instability evolves; and 4) the enhanced mixing produced by the coherent mode.

2.1 *Time-Averaged Base Flow*

Consider the two-dimensional streaming flow of a compressible fluid past an airfoil of length L. The pertinent situation arises at angles of attack at which (absent intervention) the flow breaks away from the suction side of the airfoil an order L distance downstream of the leading edge. Let U_s, R_s, P_s and μ_s denote the characteristic speed, density, static pressure and dynamic viscosity along the separating streamline, respectively. A subsonic adiabatic flow is assumed and, since the analysis to follow is limited to a small neighborhood of the separating streamline, the pressure–density relation $P = R^\gamma$ is approximated by the Chaplygin–Karman–Tsien equation of state [2, p. 285]

$$P - 1 = \gamma \frac{R-1}{R} \tag{1}$$

where pressure P and density R are non-dimensionalized by P_s and R_s, respectively, and γ is the ratio of specific heats. Equation (1), which is just a tangent approximation to the exact pressure–density relation, greatly simplifies the analysis by allowing use of the hodograph method.

The limiting form of the flow field on the airfoil scale as the Reynolds number $Re \equiv R_s U_s L / \mu_s$ tends to infinity can then be found in the class of potential flows described by a generalized version of Kirchhoff's free-streamline
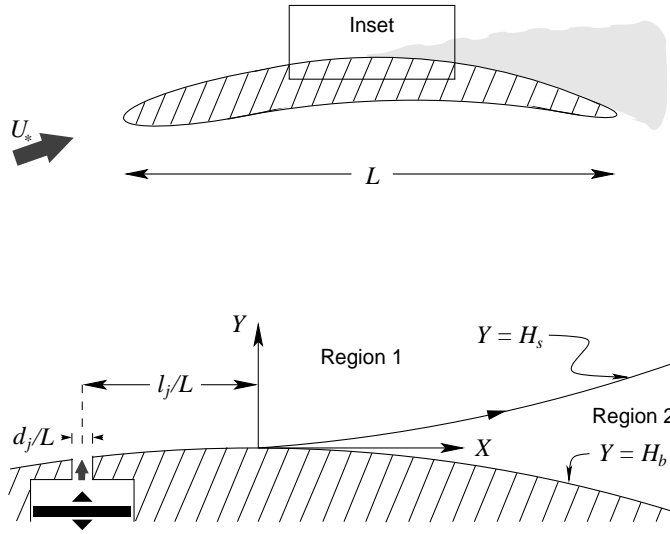
Figure 1. Separated flow configuration.

theory [3]. The solutions are parameterized by the point of intersection between the airfoil surface and the free-streamline that separates the oncoming flow from the stagnant fluid in the recirculation zone, i.e. regions 1 and 2 of figure 1, respectively. References [4] and [5] show how the exact location of this separation point depends on the detailed nature of the viscous flow along the airfoil surface.

The base-flow separation point is left unspecified at present, but it is assumed that both the site of fluid-injection and the onset of shear-layer roll-up lie within a short distance (relative to L) of that point. Accordingly, it suffices to give the base-flow solution only in the vicinity of its separation point which is now taken as the origin of the Cartesian coordinate system $\{X, Y\} \equiv \boldsymbol{X}$ with X and Y tangent and normal, respectively, to the surface (cf. figure 1) and both non-dimensionalized by L.

The Kirchhoff theory, when generalized to compressible fluids satisfying (1), predicts the shape of the free streamline separating regions 1 and 2 to be

$$Y = H_s(X) = aX^{3/2} + bX^2 + O(X^{5/2}) \tag{2}$$

for $0 < X \ll 1$, where a is a constant that depends on the viscous flow along the surface and b is half the non-dimensionalized airfoil curvature at $X = 0$. References [4] and [5] show that for high-Reynolds-number separations from a smooth surface $0 < a \leqslant O(1)$. The separations of interest here result from the action of an adverse pressure gradient so $b < 0$ and, to required order of accuracy, the airfoil shape is

$$Y = H_b(X) = bX^2 + O(X^3) \tag{3}$$

for $|X| \ll 1$.

In region 1, the base-flow velocity (non-dimensionalized by U_s) is given as

$$\boldsymbol{U}_1 = \{U_1, V_1\} = \hat{\boldsymbol{\imath}} + \frac{\mathrm{d}\Phi_1}{\mathrm{d}\boldsymbol{X}}, \tag{4}$$

with velocity potential

$$\Phi_1 = -\frac{a}{\sqrt{1 - M_s^2}} \mathrm{Re}\left(\mathrm{i}Z^{3/2}\right) + O(|Z|^2) \tag{5}$$

for $|\boldsymbol{X}| \ll 1$, where $\hat{\boldsymbol{\imath}}$ is the unit vector in the X direction, $\mathrm{i} \equiv \sqrt{-1}$, $Z \equiv X + \mathrm{i}\sqrt{1 - M_s^2}\,Y$, $M_s \equiv U_s/\sqrt{\gamma P_s/R_s}$ is the characteristic Mach number along the free streamline and a numeric subscript on a dependent variable indicates

the flow region to which it applies. Corresponding expressions for the region 1 density and pressure can be found from (1) and the appropriate Bernoulli equation, eg.

$$P_1 = 1 + \gamma M_s^2 (1 - U_1) + O(|Z|).$$

In region 2, the velocity vanishes and the density and pressure take on their constant free-streamline values.

3 Linear Unsteady Flow Field

The unsteady fluid motion generated by the surface injection (but external to the actuation device) introduces an additional length scale U_s/ω_j into the problem where ω_j is a characteristic angular injection frequency. In flow-control theory, it is usual to work in terms of a reduced frequency (or Strouhal number), eg. $F^+ \equiv \omega_j L/2\pi U_s$. Values of reduced frequency reported in the literature vary widely however, for flow-control approaches where mixing enhancement is the active mechanism, F^+ is approximately order one. (At higher reduced frequencies, effective flow control is thought to result from virtual aeroshaping.) In the following analysis

$$\mathcal{F}(Re) \ll \epsilon \equiv \frac{U_s/\omega_j}{L} = \frac{1}{2\pi F^+} \ll 1 \tag{6}$$

is assumed where the lower limit is introduced so that viscous effects are for the most part passive. The precise form of $\mathcal{F}$ depends on the detailed nature of the viscous flow along the airfoil surface, eg. $\mathcal{F} = Re^{-1/4}$ in the case of laminar separation.

Minimization of parasitic losses is a primary concern in the design of efficient flow-control systems. With this in mind, the injection strength (measured in terms of net momentum flux, say) is assumed sufficiently small for the unsteady dynamics to remain predominantly linear at least within an order U_s/ω_j neighborhood of the base-flow separation point. The unsteady-flow field is then characterized by time scale t non-dimensionalized by ω_j and includes a spatial variation on the scale $\boldsymbol{x} \equiv \boldsymbol{X}/\epsilon$ which is short compared to the airfoil chord.

It follows from these considerations that the velocity field (external to the actuation device and non-dimensionalized by U_s) can be expressed as

$$\boldsymbol{u}_i = \delta_{i1} \boldsymbol{U}_1 + \boldsymbol{\nabla} \left[\phi_i + \delta_{i1} M_s^2 \left(\frac{\partial}{\partial t} + \frac{\partial}{\partial x} \right) (\Phi_1 \phi_1) \right] \tag{7}$$

for $i = 1, 2$, with potentials ϕ_i governed by

$$\left[M_s^2 \left(\frac{\partial}{\partial t} + \delta_{i1} \frac{\partial}{\partial x} \right)^2 - \nabla^2 \right] \phi_i = 0 \tag{8}$$

where δ_{ij} is the Kronecker delta function, $\boldsymbol{\nabla} \equiv \mathrm{d}/\mathrm{d}\boldsymbol{x}$ and similar expansions apply for the density and pressure. Equation (8) must be solved subject to slip or injection conditions on the airfoil surface $\epsilon y = H_b$ as well as appropriate far-field conditions as $y \to \infty$.

Solutions in regions 1 and 2 are, of course, coupled by kinematic and dynamic conditions at the free streamline. Upon eliminating the unsteady perturbation to H_s and expressing the result in terms of ϕ_i these conditions become, to required order of accuracy,

$$\frac{\partial}{\partial y} \left[\frac{\partial}{\partial t} \phi_1 - \left(\frac{\partial}{\partial t} + \frac{\partial}{\partial x} \right) \phi_2 \right] = \mathcal{L}_K \left(\phi_1, \phi_2; \epsilon^{-1} H_s, H_s', \epsilon H_s'', M_s^2 \right), \tag{9}$$

$$\frac{\partial}{\partial t} \left[\left(\frac{\partial}{\partial t} + \frac{\partial}{\partial x} \right) \phi_1 - \frac{\partial}{\partial t} \phi_2 \right] = \mathcal{L}_D \left(\phi_1, \phi_2; \epsilon^{-1} H_s, H_s', \epsilon H_s'', M_s^2 \right), \tag{10}$$

at $\epsilon y = H_s$ for $x > 0$, where $\mathcal{L}_K$ and $\mathcal{L}_D$ are linear operators on ϕ_i (see appendix) and a prime denotes differentiation with respect to X.

The linear nature of the unsteady problem is now exploited by expressing the solution as the sum of two components: one directly forced by, but external to, the actuator and the other excited along the separating shear layer by the Kelvin–Helmholtz mechanism. Both components are, of course, ultimately related to the surface injection, but the (artificial) splitting is used here to simplify the subsequent analysis by isolating the distinct spatial scales on which the unsteady flow evolves.

3.1 *Forced Solution*

Reference [6] shows that small-amplitude unsteady injection along a flat plate over which a high-Reynolds number flow passes gives rise to both acoustic and hydrodynamic modes of motion. The latter is confined to the thin viscous layer adjacent to the surface and takes the form of Tollmien–Schlichting waves. The T–S waves will grow as they propagate downstream if the injection frequency lies within the unstable band dictated by the local boundary-layer profile. The assumption employed here and embodied in (6) and (7) is that only the acoustic motion persists at order U_s/ω_j distances from the injection site, i.e. that ω_j is less than the so-called lower branch frequency.

Attention is focussed on injections through two-dimensional slots of width d_j placed a distance ℓ_j upstream of the base-flow separation point (cf. figure 1) where typical values encountered in synthetic and pulsed jet flow-control experiments suggest $d_j \ll \ell_j$ with ℓ_j order U_s/ω_j. For simplicity, the injection is assumed to be normal to the airfoil surface with a monochromatic velocity of period $2\pi/\omega_j$. More complicated injections can always be obtained by superposition.

The leading-order outward propagating solution to (8) in region 1 is then

$$\phi_1^f \sim \frac{1}{8}\frac{1}{\sqrt{1-M_s^2}}\frac{d_j\omega_j}{U_s}\left(\mathrm{i}-\frac{\partial}{\partial t}\right)\bar{v}_j\left(t+M_s^2\frac{x-x_j}{1-M_s^2}\right)\mathrm{H}_0^{(1)}\left(M_s\frac{|z-x_j|}{1-M_s^2}\right)+\text{c.c.} \tag{11}$$

where superscript f indicates the forced component, $\bar{v}_j(t)$ is the area-averaged slot exit velocity non-dimensionalized by U_s, $\mathrm{H}_0^{(1)}$ is the Hankel function of the first kind and zero-th order, $z \equiv Z/\epsilon$ and $x_j \equiv -\ell_j\omega_j/U_s$.

The right-hand sides of (9) and (10) give rise to an order $\epsilon^{1/2}$ correction to (11) which, owing to the behavior of H_s'', becomes singular as $|x| \to 0$. It is the removal of this singularity by application of an unsteady Kutta condition that provides the coupling between the forced and excited components of motion.

3.2 *Excited Solution*

The component of unsteady fluid motion excited along the separating shear layer is more strongly dependent on the flow in the recirculation zone than the forced component. It is only when the transverse extent of region 2 becomes order U_s/ω_j that the mechanism responsible for the excited motion takes on the classic Kelvin–Helmholtz instability form. Equations (2) and (3) show that this stage is reached when X becomes order $(\epsilon/a)^{2/3}$ at which point the excited solution varies (locally) on the x scale.

As indicated above, the coupling between the forced and excited solutions takes place near the base-flow separation point as $|x| \to 0$. It is therefore necessary to determine the excited solution over the streamwise scale $x_1 = (a/\epsilon)^{2/3}X$ where the curvature of the base-flow free streamline becomes important. If the dynamics remain linear on the x_1 scale, the uniformly valid solution to (8) in region 1 has the form

$$\phi_1^e \sim \mathbb{A}(x_1)\exp\left[\mathrm{i}(a^2\epsilon)^{-1/3}\int_0^{x_1}\alpha(\xi)\mathrm{d}\xi-\kappa_1\left(y-\epsilon^{-1}H_s\right)-\mathrm{i}t\right]+\text{c.c.} \tag{12}$$

for $x_1 > 0$, where superscript e indicates the excited component, the slowly varying amplitude function $\mathbb{A}$ is determined by a solvability condition at next order (cf. figure 2) and c.c. denotes the complex conjugate. The slowly varying wavenumber $\alpha(x_1)$ is determined by the well-known characteristic equation describing the Kelvin–Helmholtz instability of a compressible vortex sheet near a solid boundary [7] which in the present notation reads

$$(1-\alpha)^2\kappa_2\tanh\left(\kappa_2\frac{H_s-H_b}{\epsilon}\right)+\kappa_1=0 \tag{13}$$

where $\kappa_i \equiv \sqrt{\alpha^2-M_s^2(1-\delta_{i1}\alpha)^2}$ with branch cuts fixed by boundedness and propagation considerations in the respective regions.

The root to (13) of relevance here is the one that yields a spatially growing downstream propagating instability wave, i.e. the root with $\operatorname{Re}\alpha > 0$ and $\operatorname{Im}\alpha < 0$ (cf. figure 3). The expansion of the corresponding eigenfunction (to which (12) represents the leading-order term) breaks down as x_1 becomes small and it is necessary to analyze the flow in an inner region where $|X|$ is order $(a\epsilon^2)^{2/3}$ and the dynamics are quasi steady. The leading-order inner-region solution turns out to have a singularity at the origin of the same form as that exhibited by the forced component.
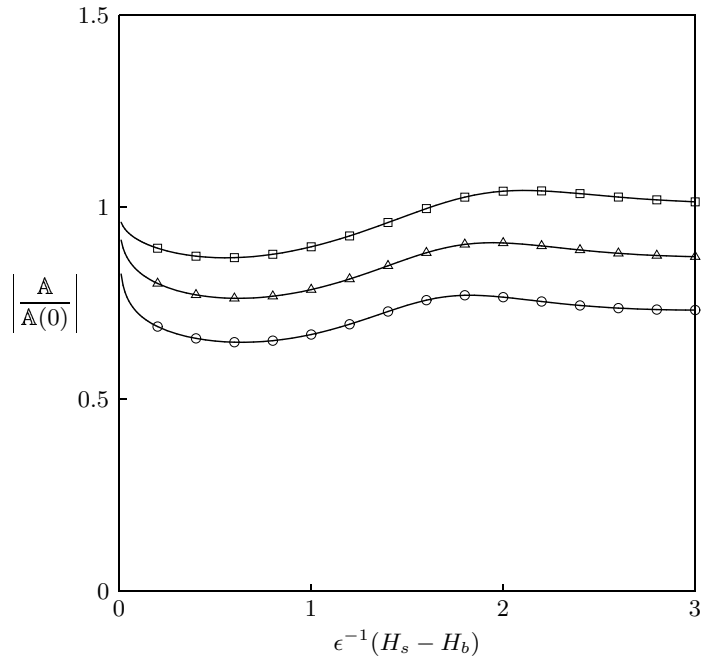
Figure 2. Slowly varying instability-wave amplitude as function of scaled region 2 thickness. $\square$, $M_s = 0.2$; $\triangle$, $M_s = 0.6$; $\ominus$, $M_s = 0.8$.
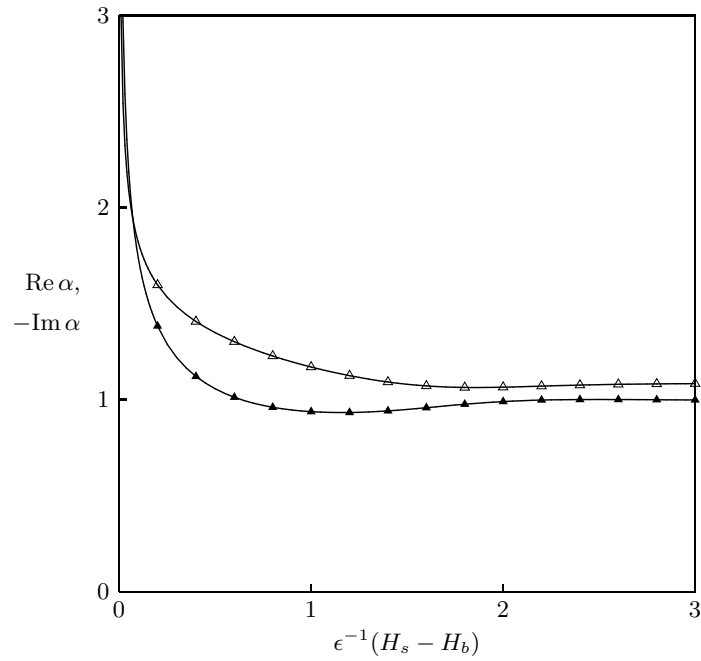

Figure 3. Unstable root to (13) at $M_s = 0.6$ as function of scaled region 2 thickness. Open symbols, $\mathrm{Re}\,\alpha$; filled symbols, $-\mathrm{Im}\,\alpha$.

The analysis of reference [8] is used here to conclude that viscous (and interactive) effects act locally to smooth out the combined singularities of the complete flow (i.e. steady base flow plus forced and excited unsteady components) such that when viewed on the comparatively large scale of the inner region the singularities of the forced and excited solutions exactly cancel. The result is an unsteady Kutta condition that relates the instability wave amplitude $\mathbb{A}$ to the surface injection as follows

$$\mathbb{A}(0) = \frac{3}{128} \frac{1}{M_s^2 \sqrt{1-M_s^2}} \frac{d_j}{L} \frac{\mathbb{L}_j}{L} \left(\frac{M_s^2 a}{1-M_s^2} \frac{L}{\ell_j}\right)^{4/3} \mathcal{G}\left(M_s \frac{|x_j|}{1-M_s^2}\right) \tag{14}$$

where

$$\mathcal{G}(\omega) \equiv \omega^{1/3} \mathrm{e}^{-\mathrm{i}(M_s\omega - \pi/3)} \left[\left(1 + \mathrm{i}\frac{1+M_s^2}{M_s}\omega\right) \mathrm{H}_0^{(1)\prime}(\omega) + \left(3 - 2M_s^2 + M_s^4\right) \omega \mathrm{H}_0^{(1)}(\omega)\right]$$

and $\mathbb{L}_j$ is the stroke length based on the area-averaged injection velocity, i.e. the length of the slug of fluid pushed from the slot during the discharge stroke.

4 Mixing Enhancement

The exponential growth of the excited component of unsteady motion causes it to dominate the forced component downstream of separation. This rapid growth continues until nonlinear effects come into play to produce a spatial equilibration as the instability wave rolls up into a discrete vortex [9]. It is generally believed that such linear instability waves are the progenitors of the large-scale coherent structures which dominate the spatial development of transitional and turbulent shear flows.

Interest here is in the effect injection-induced large-scale coherent structures have on momentum transfer across the separating shear layer. A time-averaged measure of the fluid entrained by the shear layer is provided by the mean shear-layer momentum thickness $\delta(s)$ where s is the downstream distance along the centerline and both s and δ are non-dimensionalized by L. The conservation equations for the mean (i.e. Reynolds averaged) motion then show that the growth in δ caused by viscous diffusion is augmented by Reynolds stresses due to both fine-grained turbulence and large-scale coherent structures.

4.1 *Mean-Flow Spreading Rate*

Reference [10] presents a high-Reynolds-number, energy-transfer-based evolutionary model for the mean-flow spreading rate $\mathrm{d}\delta/\mathrm{d}s$ that includes effects due to viscous dissipation and the production of and interaction between coherent modes and fine-grained turbulence. The transverse integrals of the Reynolds-stress terms which appear in the model are evaluated by exploiting the ability of local linear inviscid stability theory to accurately predict the fast-scale propagation and cross-stream distribution of the coherent structures even in the presence of turbulence. The corresponding amplitudes are however determined by nonlinear considerations on the s scale.

The most rapid rise in spreading rate (and hence entrainment) occurs downstream of the linearly unstable region where viscous diffusion gives rise to a $\sqrt{s}$ growth in δ, but upstream of the vortex-merging stage where fine-grained-turbulence production leads to a linear growth in δ. For a monochromatic coherent-mode in the intermediate streamwise region, the evolutionary spreading-rate model simplifies to

$$\bar{I}\frac{\mathrm{d}\delta}{\mathrm{d}s} = |A|^2\tilde{I}_{rs}, \qquad \bar{\tilde{I}}\frac{\mathrm{d}\delta|A|^2}{\mathrm{d}s} = |A|^2\tilde{I}_{rs}, \tag{15}$$

where $A(s)$ is a nonlinear amplitude function based on appropriately normalized eigenfunctions from linear stability theory, $\bar{I}$ is the mean-flow kinetic-energy flux integral, $\bar{\tilde{I}}$ is the time-mean of the kinetic-energy flux integral for the coherent mode and $|A|^2\tilde{I}_{rs}$ gives the energy exchange rate between the mean flow and coherent mode. The flux integrals $\bar{I}$ and $\bar{\tilde{I}}$ are constants while $\tilde{I}_{rs}$ is a function of δ [10]. The latter is approximated here as

$$\tilde{I}_{rs} \approx C\delta - D\delta^2$$

where, in general, C and D depend on s. Equations (15) are integrated to yield

$$\frac{\delta_\infty - \delta}{\delta_\infty - \delta_0} = \frac{\delta_\infty |A_\infty|^2 - \delta|A|^2}{\delta_\infty |A_\infty|^2 - \delta_0|A_0|^2} \tag{16}$$
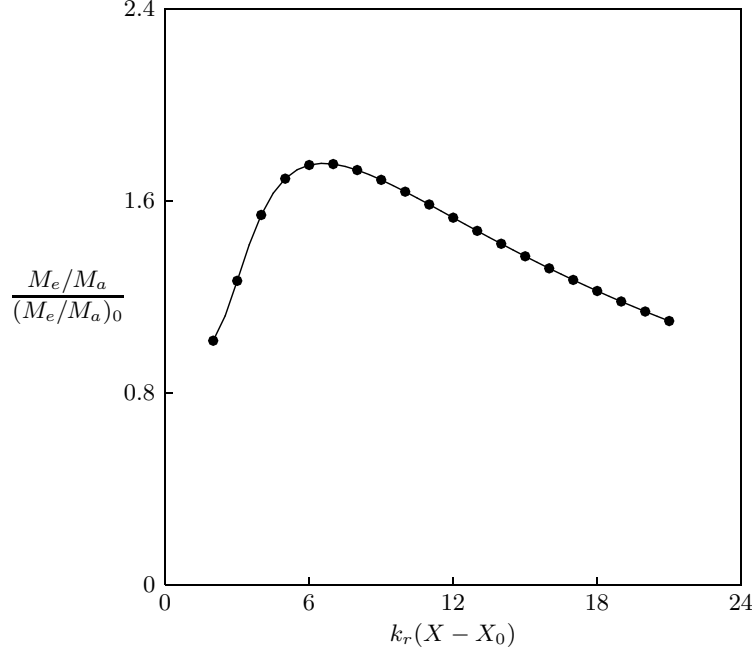
Figure 4.   Normalized flow-control metric as function of scaled downstream distance with $\varepsilon = 0.006$, $\vartheta = 0.25$ and $k_r X_0 = 9$.

and

$$\delta|A|^2 = \frac{\delta_0|A_0|^2\delta_\infty|A_\infty|^2}{\delta_0|A_0|^2 + \left(\delta_\infty|A_\infty|^2 - \delta_0|A_0|^2\right)\exp\left(-2\int_{s_0}^{s}k_r\,\mathrm{d}\sigma\right)} \tag{17}$$

where $k_r \equiv \delta_\infty|A_\infty|^2 D/2\bar{I}$ is an s dependent local linear growth rate, $\delta_\infty|A_\infty|^2 \equiv \delta_0|A_0|^2 + (\delta_\infty - \delta_0)\bar{I}/\bar{\bar{I}}$ and $\delta_\infty \equiv C/D$ are equilibration values that depend on both frequency and Reynolds number and subscript 0 indicates evaluation at a streamwise location s_0 near the end of the linearly unstable region.

4.2   *Flow-Control Metric*

The degree to which the injection induced mixing enhancement effects separation control is quantified using a premise presented in reference [1]. Accordingly, the oncoming flow re-attaches to the airfoil if and when the mass of fluid entrained into the shear layer exceeds that available for entrainment, i.e. the fluid in the recirculation zone. The amount of mass entrained M_e over an arbitrary downstream distance is proportional to the integral of δ over the corresponding distance along the shear-layer center line while the amount of mass available M_a is proportional to the corresponding volume of region 2.

To significantly impact airfoil performance, the re-attachment must occur a short distance (relative to chord) downstream of the separation point. Consequently, the small-X approximation is made and $s = X + O(X^4)$. If it is further supposed that k_r is effectively constant over the region of interest then it follows from (2), (3), (16) and (17) that the flow-control measure of merit is

$$\frac{M_e}{M_a} \propto \frac{5\delta_\infty}{4ak_r}\frac{(1-\varepsilon)2k_r(X-X_0) + (1-\vartheta)\ln\left\{\varepsilon + (1-\varepsilon)\exp[-2k_r(X-X_0)]\right\}}{(1-\varepsilon)(X^{5/2} - X_0^{5/2})} \tag{18}$$

where $\varepsilon \equiv \delta_0|A_0|^2/\delta_\infty|A_\infty|^2$ and $\vartheta \equiv \delta_0/\delta_\infty$ are disturbance-energy and mean shear-layer thickness parameters, respectively.
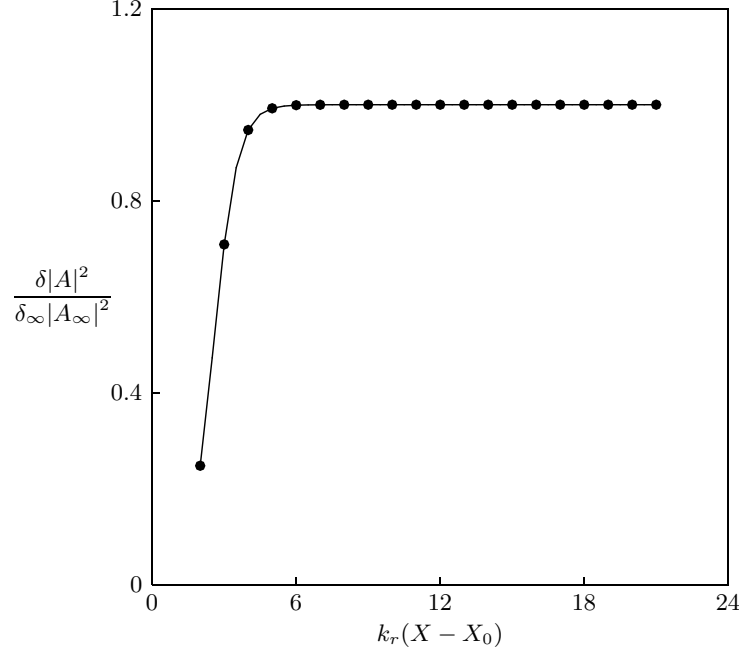
Figure 5. Normalized disturbance energy as function of scaled downstream distance with $\varepsilon = 0.006$.

5 Results and Conclusions

The flow-control metric determined by (18) is plotted in figure 4 in normalized form for values of ε, ϑ and $k_r X_0$ estimated from the experimental data considered in reference [9]. The figure reveals the competition between shear-layer entrainment and recirculation-zone expansion as the flow evolves downstream of separation. At small abscissa, the shear-flow spreading rate exceeds the rate of recirculation-zone expansion and the flow-control metric increases. This trend continues until the instability wave roll-up and spatial equilibration are complete (cf. figure 5). The enhanced mixing generated by the coherent mode is then maximal and further recirculation-zone growth results in a decline in the flow-control metric. Accounting for vortex merging and its attendant fine-grained turbulence production which are dominant at the larger downstream distances merely alters the rate of decline. Overall the curve in figure 4 is in good agreement with the experimental data presented in reference [1, fig. 4].

Under the premise employed here, successful separation control results when the ratio M_e/M_a exceeds unity. The location of the peak in figure 4 is decisive. In this regard, it should be noted that both abscissa and ordinate depend implicitly on the fluid injection parameters. In the simplest approximation, k_r is given by the linear weakly non-parallel analysis of §3.2, so

$$k_r(X - X_0) \approx -\operatorname{Im}\alpha(\infty)\frac{\omega_j L}{U_s}(X - X_0),$$

and the abscissa is proportional to a reduced frequency $f^+ = F^+(X - X_0)$ based on the streamwise length of the recirculation zone. The peak in M_e/M_a is then suggestive of an optimal injection frequency, however the dependence on X_0 means that the optimum is not global. The normalization $(M_e/M_a)_0$ used for the ordinate is proportional to the ratio of shear-layer to recirculation-zone thickness at $X = X_0$ and thus varies as $1/X_0$. Shifting the onset of nonlinearity upstream (i.e. reducing X_0) increases the likelihood of flow re-attachment.

The quantity X_0 is determined by the properties of the instability wave from which the coherent mode originates. It can be reduced by increasing either the initial linear instability wave amplitude or frequency. Relating X_0 to the *injection* parameters is, however, complicated by the coupling condition (14) which shows that the initial linear amplitude $\mathbb{A}(0)$ involves its own frequency dependence. Figure 6 is a plot of $|\mathbb{A}(0)|$ as a function of frequency for various M_s. It follows that X_0 decreases with slot width d_j and stroke length $\mathbb{L}_j$, increases with distance between

$$\left(\frac{\ell_j}{aL}\right)^{4/3}\frac{|\mathbb{A}(0)|}{d_j\mathbb{L}_j/L^2}$$
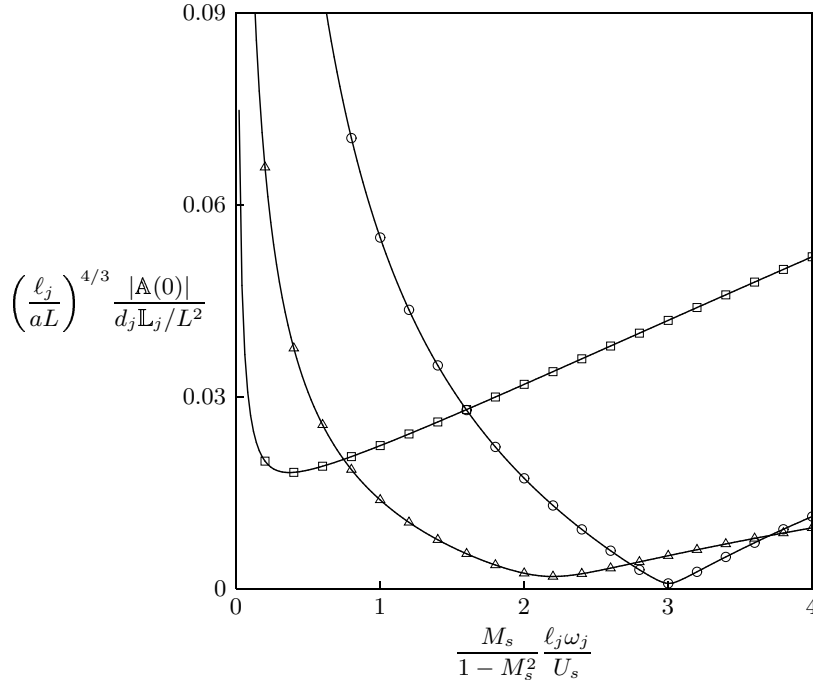
$$\frac{M_s}{1-M_s^2}\frac{\ell_j\omega_j}{U_s}$$

Figure 6.   Initial instability-wave amplitude as function of injection frequency. $\square$, $M_s = 0.2$; $\triangle$, $M_s = 0.6$; $\ominus$, $M_s = 0.8$.

injection site and separation point ℓ_j and can either increase or decrease with non-dimensional injection frequency $\ell_j\omega_j/U_s$.

Clearly, even in the context of the foregoing simplifications, the flow-control metric (18) involves an intricate dependence on the fluid injection parameters. This may explain the wide range of reported frequencies at which unsteady surface injection successfully delays or prevents flow separation. Understanding this parametric dependence is necessary in order to guide the optimization of actuator design for maximal flow-control effectiveness while accurately capturing it in a deterministic-stress model is a prerequisite for performing system-level numerical predictions using steady-flow design codes.

REFERENCES

[1] D. GREENBLATT and I. J. WYGNANSKI 2000 *Progress in Aerospace Sciences* **36**, 487–545. The control of flow separation by periodic excitation.

[2] C. S. YIH 1969 *Fluid Mechanics*. New York: McGraw–Hill.

[3] M. I. GUREVICH 1965 *Theory of Jets in Ideal Fluids*. New York: Academic.

[4] V. V. SYCHEV 1972 *Izvestiya Akademii Nauk SSSR, Mekhanika Zhidkosti i Gaza* (3), 47–59. (Engl. transl. *Fluid Dynamics* **7**(3) 407–417.) Laminar Separation.

[5] Vik. V. SYCHEV 1987 *Izvestiya Akademii Nauk SSSR, Mekhanika Zhidkosti i Gaza* **3**, 51–60. (Engl. transl. *Fluid Dynamics* **22**(3) 371–379.) Theory of Self-Induced Separation of a Turbulent Boundary Layer.

[6] X. WU 2002 *Journal of Fluid Mechanics* **453**, 289–313. Generation of sound and instability waves due to unsteady suction and injection.

[7] S.-I. PAI 1954 *Journal of Aeronautical Sciences* **21**(5), 325–328. On the Stability of a Vortex Sheet in an Inviscid Compressible Fluid.

[8] M. E. GOLDSTEIN 1984 *Journal of Fluid Mechanics* **145**, 71–94. Generation of instability waves in flows separating from smooth surfaces.

[9] L. S. HULTGREN 1992 *Journal of Fluid Mechanics* **236**, 635–664. Nonlinear spatial equilibration of an externally excited instability wave in a free shear layer.

[10] J. T. C. LIU 1989 *Annual Review of Fluid Mechanics* **21**, 285–315. Coherent Structures in Transitional and Turbulent Free Shear Layers.

Appendix

The linear operators on the right-hand sides of (9) and (10) are given as

$$\mathcal{L}_K \equiv \left[H'_s \frac{\partial}{\partial x} - \epsilon^{-1} H_s H'_s M^2_s \left(\frac{\partial}{\partial t} + \frac{\partial}{\partial x} \right) \frac{\partial}{\partial y} - \epsilon H''_s M^2_s \right] \frac{\partial}{\partial t} \phi_1 - \left[H'_s \left(\frac{\partial}{\partial t} + 2\frac{\partial}{\partial x} \right) + \epsilon H''_s \right] \frac{\partial}{\partial x} \phi_2,$$

and

$$\mathcal{L}_D \equiv - \left[H'_s \frac{\partial}{\partial y} + \epsilon^{-1} H_s H'_s M^2_s \left(\frac{\partial}{\partial t} + \frac{\partial}{\partial x} \right)^2 \right] \frac{\partial}{\partial t} \phi_1 - \epsilon H''_s \frac{\partial}{\partial y} \phi_2,$$

to required order of accuracy.

REPORT DOCUMENTATION PAGE

Form Approved
OMB No. 0704-0188

Public reporting burden for this collection of information is estimated to average 1 hour per response, including the time for reviewing instructions, searching existing data sources, gathering and maintaining the data needed, and completing and reviewing the collection of information. Send comments regarding this burden estimate or any other aspect of this collection of information, including suggestions for reducing this burden, to Washington Headquarters Services, Directorate for Information Operations and Reports, 1215 Jefferson Davis Highway, Suite 1204, Arlington, VA 22202-4302, and to the Office of Management and Budget, Paperwork Reduction Project (0704-0188), Washington, DC 20503.

1. AGENCY USE ONLY (*Leave blank*)	2. REPORT DATE July 2004	3. REPORT TYPE AND DATES COVERED Final Contractor Report

4. TITLE AND SUBTITLE

Injection Induced Mixing in Flows Separating From Smooth Surfaces

6. AUTHOR(S)

David W. Wundrow

5. FUNDING NUMBERS

Independent Research Fund
22 IRD00002
NCC3–1070

7. PERFORMING ORGANIZATION NAME(S) AND ADDRESS(ES)

Ohio Aerospace Institute
22800 Cedar Point Road
Brook Park, Ohio 44142

8. PERFORMING ORGANIZATION REPORT NUMBER

E–14667

9. SPONSORING/MONITORING AGENCY NAME(S) AND ADDRESS(ES)

National Aeronautics and Space Administration
Washington, DC 20546–0001

10. SPONSORING/MONITORING AGENCY REPORT NUMBER

NASA CR—2004–213176

11. SUPPLEMENTARY NOTES

Project Manager, John J. Adamczyk, Research and Technology Division, NASA Glenn Research Center, organization code 5000, 216–433–5829.

12a. DISTRIBUTION/AVAILABILITY STATEMENT

Unclassified - Unlimited
Subject Category: 34   Distribution: Nonstandard

Available electronically at http://gltrs.grc.nasa.gov

This publication is available from the NASA Center for AeroSpace Information, 301–621–0390.

12b. DISTRIBUTION CODE

13. ABSTRACT *(Maximum 200 words)*

An analytic model for predicting the effect of unsteady local surface injection on the flow separating from a streamlined body at angle of attack is proposed. The model uses the premise that separation control results from enhanced mixing along the shear layer that develops between the main stream and the fluid in the underlying recirculation zone. High-Reynolds-number asymptotic methods are used to connect the unsteady surface injection to an instability wave propagating on the separating shear layer and then to the large-scale coherent structures that produce the increased mixing. The results is a tool that can guide the choice of fluid-actuator parameters to maximize flow-control effectiveness and may also facilitate computer-based numerical experiments.

14. SUBJECT TERMS

Boundary layer separation; Fluid injection; Mixing; Adaptive control; High Reynolds number; Asymptotic methods; Mathematical models

15. NUMBER OF PAGES
17

16. PRICE CODE

17. SECURITY CLASSIFICATION OF REPORT	18. SECURITY CLASSIFICATION OF THIS PAGE	19. SECURITY CLASSIFICATION OF ABSTRACT	20. LIMITATION OF ABSTRACT
Unclassified	Unclassified	Unclassified	

NSN 7540-01-280-5500

Standard Form 298 (Rev. 2-89)
Prescribed by ANSI Std. Z39-18
298-102